

Spiral shocks, triggering of star formation and the velocity dispersion in Giant Molecular Clouds

I. A. Bonnell^{1*}, C.L. Dobbs¹, T. P. Robitaille¹ & J.E. Pringle²

¹ *School of Physics and Astronomy, University of St Andrews, North Haugh, St Andrews, Fife, KY16 9SS.*

² *Institute of Astronomy, Madingley Road, Cambridge, CB3 0HA*

16 July 2018

ABSTRACT

We present numerical simulations of the passage of gas through a galactic spiral shock and the subsequent formation of giant molecular clouds (GMCs), and the triggering of star formation. In these simulations, we take account of the observed inhomogeneity, or clumpiness, of the pre-shock interstellar medium. As might be expected, the spiral shock forms dense clouds while dissipating kinetic energy, producing regions that are locally gravitationally bound and collapse to form stars. But the effect of the clumpiness of gas as it passes through the shock is to generate chaotic internal motions in the gas. The kinematics of these motions are found to agree with the observed velocity-dispersion/size relation found in star-forming regions. In contrast to the standard picture where continuously driven turbulence generates the density inhomogeneities in star-forming clouds, we find here that it is the clumpiness of the interstellar gas that produces the chaotic motions as it passes through the spiral shock and initiates the star formation process. The velocity dispersion can be understood as being due to the random mass loading of clumps as they converge in the spiral shock. Within these clouds both the timescale for the decay of these motions, and the timescale for forming stars, are comparable to the clouds' dynamical lifetimes. In this model there is no need for any internal or external continuous driving mechanism for the 'turbulence'. In addition, the coupling of the clouds' internal kinematics to their externally triggered formation removes the need for the clouds to be self-gravitating. Indeed, while clearly some parts of the clouds are self-gravitating and able to form stars, most of the molecular material remains gravitationally unbound. This can provide a simple explanation for the low efficiency of star formation.

Key words: stars: formation — galaxies: ISM — ISM: clouds — galaxies: star clusters — galaxies: kinematics and dynamics — open clusters and associations: general.

1 INTRODUCTION

Our understanding of the star formation process has recently undergone a paradigm shift from the earlier quasi-static picture where the environment plays no role, to an awareness that star formation is an extremely dynamical process where the local environment, and interactions, play a dominant role in determining the resultant stellar properties (Hartmann et al. 2001; Larson 2003; Mac Low & Klessen 2004; Bonnell et al. 2001). Traditionally, giant molecular clouds (GMCs), the sites of star formation, were thought to be long-lived entities (ages > 10 dynamical times) in order to explain the low star formation rate in our Galaxy (Zuck-

erman & Evans 1974; Blitz & Shu 1980; Leisawitz 1990). Recently, it has become clear that observational evidence from young stellar populations implies a relatively fast star formation process whereby clouds appear, form stars and then disperse on their local dynamical times of a few million years (Elmegreen 2000; Hartmann et al. 2001). One of the basic properties of these clouds is that they display internal chaotic motions which are highly supersonic. These motions are usually interpreted as 'turbulence', and observations suggest that any driving of the observed turbulence should come from the largest scales of the GMC (Brunt 2003). A succession of numerical simulations (Mac-Low et al., 1998; Padoan & Nordlund, 1999; Ostriker, Gammie & Stone, 1999) have demonstrated that such supersonic motions, in the absence of some continuous driving mechanism, dissipate on

* E-mail: iab1@st-and.ac.uk

one or two dynamical timescales. The realisation that the lifetimes of these clouds are comparatively short then suggests that the formation mechanism for GMCs is a dynamical one (Roberts 1969; Shu et al. 1972; Pringle et al. 2001). One implication of such a mechanism is that gravitational clouds need not control their own evolution in the sense that, contrary to the usual assumption, they need not be self-gravitating entities (although of course some parts of them do need to be in order to form stars), nor in virial equilibrium. Thus the internal motions which we see may be kinematic, rather than dynamic (Pringle et al. 2001). If molecular clouds are globally gravitationally unbound, the perceived problems of their low star formation efficiencies and supposed long lifetimes are erased (Elmegreen 2000). Recent simulations of unbound molecular clouds have shown how star formation can proceed while the majority of the gas escapes due to its excess kinetic energy (Clark & Bonnell 2004; Clark et al. 2005).

Star formation has long been known to occur primarily in the spiral arms of disc galaxies (Baade 1963). Spiral arms are denoted by the presence of young stars, HII regions, dust and giant molecular clouds, all signatures of the star formation process (van den Bergh 1964; Schweizer 1976; Bash, Green & Peters 1977; Elmegreen & Elmegreen 1983; Rumsay & Kaufman 1983; Ferguson et al. 1998). What is still unclear is the exact role of the spiral arms in inducing the star formation. Is it simply that the higher surface density due to the orbit crossing is sufficient to initiate star formation, as in a Schmidt law, or do the spiral arms play a more active role? Roberts (1969) suggested that the spiral shock that occurs as the gas flows through the potential minima triggers the star formation process in spiral galaxies. Shock dissipation of excess kinetic energy can result in the formation of bound structures which then collapse to form stars. This of course can provide the dynamical mechanism we need to form the observed molecular clouds. The formation of giant molecular clouds in spiral arms can occur in one of two ways (e.g. Blitz, & Rosolowsky 2004): through the agglomeration of smaller molecular cloudlets as they pass through the spiral arms (eg., Pringle et al. 2001) or through the formation of molecules in dense atomic gas clouds that themselves have been compressed in the spiral arms (Bergin et al. 2004, Elmegreen 1993).

In either formation scenario, we need to explain the observed properties of GMCs. GMCs are observed to contain highly supersonic motions and a wealth of structure on all length scales (Larson 1981; Blitz & Williams 1999; Elmegreen & Scalo 2004). The supersonic motions are found such that the velocity dispersion v varies with length scale R according to the relation $v \propto R^{1/2}$ (Larson 1981; Myers 1984; Miesch & Bally 1993; Heyer & Schloerb 1997; Heyer & Brunt 2004). A number of authors, on the basis on numerical simulations, argue that it is these supersonic motions, maintained by internal or external driving mechanism, which induce the observed density inhomogeneities in the gas (Mac Low & Klessen 2004; Elmegreen & Scalo 2004), and that it is therefore the supersonic motions which drive star formation. Suggested candidates for an internal driving mechanism include feedback from low-mass star formation (Silk 1985) even though GMCs with and without star formation have similar kinematic properties (Williams, Blitz & McKee 2000). External candidates include supernova and

superbubbles (Wada & Norman 2001; Elmegreen & Scalo 2004). Although there is sufficient energy in these events to explain the kinematics of the ISM and they can potentially generate the correct velocity dispersion sizescale relation (Kornreich & Scalo 2000), what is unclear is their relevance to star formation, and in particular to the triggering of star formation in spiral arms.

There are, as mentioned above, both observational and theoretical reasons for supposing that molecular cloud lifetimes are quite short (Elmegreen 2000; Pringle, Allen & Lubow 2001; Hartmann, Ballesteros-Paredes & Bergin, 2001), being at most a few dynamical, or kinematic (crossing) timescales. If this is the case, then a continuous source of turbulence is not required. Indeed, all that is required is some initial impulsive input of energy. Moreover, in this case, the motions do not need to be 'turbulent' in the usual sense, as there is barely time for energy to work its way through a cascade of eddies. What is the physical mechanism which gives rise to such an impulse? Since star formation occurs in spiral arms, the obvious place to look for such a mechanism is in the spiral arms itself.

In view of all this, we suggest here an alternative origin for the observed chaotic supersonic motions. It is well known that the interstellar medium is highly structured on all scales (Lauroesch et al. 2000; Dickey & Lockman 1990; Elmegreen & Scalo 2004). The result of passing a shock through such clumpy gas is to give rise to internal motions. The magnitude of the motions so generated depends on the degree of inhomogeneity in the pre-shock medium. We propose here that the passage of the clumpy interstellar medium through a galactic spiral shock not only produces the dense environment in which molecular clouds form (Cowie 1981; Elmegreen 1979, 1989, 1991), but also gives rise at the same time to their supersonic internal motions. We stress again that these motions are not really driven turbulence in the usual sense of energy being passed from large eddies down through a spectrum of smaller ones (Tennekes & Lumley 1972). Rather, the passage of a shock through the clumpy pre-shock medium leads to supersonic internal motions being generated at all scales simultaneously. There have been several numerical studies of the effects of spiral arms on gas flows. Some assume that the pre-shock ISM is smooth and concentrate on the generation of instabilities (e.g. Kim & Ostriker 2002). Others consider global effects of the galactic flows (Wada & Koda 2004; Gittens & Clarke 2004). Here we present numerical simulations capable of following both the galactic-scale gas dynamical response to the passage of a spiral arm and the small-scale triggering of star formation, but taking account of the inhomogeneity of the pre-shock ISM

2 CALCULATIONS

We use high resolution Smoothed Particle Hydrodynamics (SPH) (Monaghan 1992, Benz et al. 1991) simulations to follow the passage of interstellar gas through a spiral arm. The code has variable smoothing lengths in time and in space and solves for the self-gravity of the gas, when included, using a tree-code (Benz et al. 1991).

2.1 Preliminary simulations of clumpy shocks

In order to demonstrate the basic idea, we first report on calculations which compare uniform and clumpy gas clouds passing through a shock induced by a one-dimensional sinusoidal potential. These demonstrate the role played by the clumpiness of the pre-shock medium in generating the post-shock velocity dispersion. These three-dimensional simulations follow the evolution of a non-self gravitating gas through a one-dimensional potential of the form

$$\Phi = A \cos(kx), \quad (1)$$

with $k = \pi/2$ and $A = 80$ such that the potential has a minimum at $x = 2$. Thus, the dimensionless velocity associated with the potential, that is the velocity acquired by falling from the peak to the trough, is $V_{\text{pot}} = \sqrt{2 \times A} \approx 12.5V$, where V is the code units for velocity. This potential was chosen to mimic the effect of the passage through a spiral arm, but in a more controlled manner. The cloud, represented by 2×10^5 SPH particles, initially has length 3 units, width 2 units and height 2 units. It starts off centred on the peak of the potential at $x = 0$. The internal sound speed of the gas is $0.3V$, and all particles are given an initial velocity of $15V$ in the x -direction, corresponding to a Mach number of 50. The gas is assumed to remain isothermal throughout. These velocities are chosen so that the material shocks itself as it climbs out of the trough of the potential in a manner analogous to gas passing through the gravitational potential of a galactic spiral arm (see below). We carry out three simulations, one in which the pre-shock density is smooth, and two in which it is clumpy. The two clumpy runs differ in the size of the clumps, with radii of 0.1 and 0.2 respectively. Both clumpy simulations are constructed of 1000 individual clumps of 200 particles each. The clumps are bounded by an external pressure term.

In Figure 1 we show the column density distributions of the smooth and small clump simulations as they leave the potential minimum and start to shock ($t = 0.15$) and also at a later time ($t = 0.25$) when the shock is fully developed. The Mach number of the shock is ≈ 30 . We compute the post-shock velocity dispersions from the velocity component parallel to the pre-shock velocity. We average the velocity dispersion over numerous distinct regions of a given size, all centred on SPH particles with high density, and considering only particles with large densities indicating their location inside the shock. We then repeat this process on many different sizes to determine how the induced velocity dispersion depends on observed size-scale. We show these in Figure 2 for the three shock simulations at a time ($t = 0.25$) when the shock is fully developed, corresponding to the latter images in Figure 1. We see that the uniform shock produces a constant, sub-sonic velocity dispersion on all length-scales, except for those comparable to the individual particle separation. This is as expected, and demonstrates that we have enough resolution to overcome the usual SPH \sqrt{N} particle noise. This velocity dispersion is related to the SPH handling of shocks which leave a residual velocity dispersion as it is a particle based method which is thus inherently clumpy on the smallest scales.

In contrast, and as expected, the clumpy shock gives rise to a significant supersonic velocity dispersion in the post-shock gas. The post-shock velocity of a small element of gas

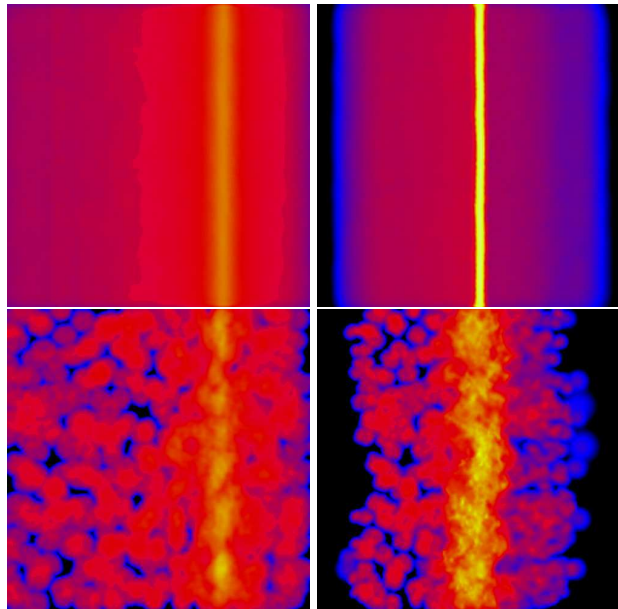


Figure 1. The column density distribution for the linear shock tests are shown for the uniform (top) and clumpy (bottom, with $r = 0.1$ clumps) gas distributions. The left panels ($1.2 < x < 3.2$, $-1 < y < 1$) show the gas as it leaves the potential minimum and begins to shock ($t = 0.15$). The right panels ($2.6 < x < 4.6$, $-1 < y < 1$) show the gas distribution when the shock is fully developed ($t = 0.25$). The logarithmic column density levels range from a minimum of 90 to a maximum of 9×10^6 in units of particles per unit area.

depends on the amount of mass it encounters, i.e., its mass loading. Conservation of momentum and the variation in the amount of mass loading due to the clumpy mass distribution thus lead to a velocity dispersion in the gas.

Within a region of size-scale less than structures in the gas, each individual parcel of gas encounters a similar column density in the shock. The uniform mass-loading then results in a zero or very small velocity dispersion. As the size-scale of the region increases, the gas samples a variation in column densities due to clumps. Then parcels of gas in the region will encounter differing amounts of mass-loading as they enter the shock and thus differing decelerations. The resulting velocity dispersion thus increases with the size of a region.

This velocity dispersion increases with the size of a region as larger regions then encounter a larger range of mass-loading in the shock. In other words, larger regions include more random samplings from the full range of mass loadings and thus post-shock velocities, resulting in a velocity dispersion which increases as $R^{1/2}$. The necessary condition being that the clumps have a significant probability of collisions in the shock. Thus, from the smallest sizes where the velocity dispersion is subsonic, the velocity dispersion increases up to sizes of twice the clump diameter, and in so doing becomes highly supersonic. On larger scales, the velocity dispersion is constant as the mass distribution is effectively uniform on these scales. The simulation with smaller clumps (larger densities) produces a higher velocity dispersion and a larger gradient than does the simulation with larger clumps, but it saturates at a smaller size scale. The lower velocity disper-

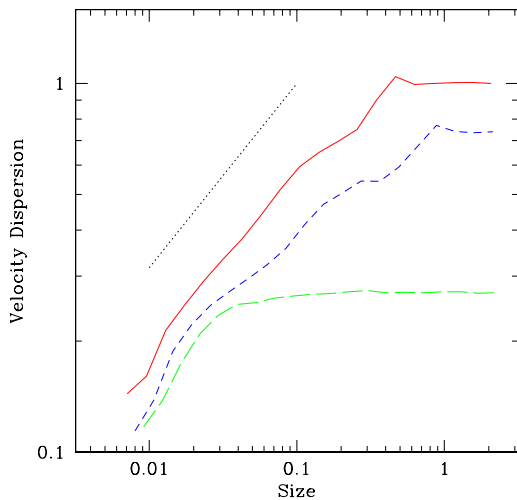


Figure 2. The one-dimensional velocity dispersion of the post-shock gas as it passes through the linear potential is plotted against size-scale for a uniform (long-dashed) and two clumpy shocks, with clumps of radii 0.1 (solid) and 0.2 (short dashed). The velocity is in units where the sound speed is 0.3 and the distance in units where the spacing between minima in the potential is 4 and the initial configuration has a maximum spatial extent of 3. The dotted-line illustrates the velocity dispersion size-scale ($v_{\text{disp}} \propto R^{1/2}$) relation deduced for molecular clouds (Larson 1981; Heyer & Brunt 2004).

sion in the larger clump simulation is due to the increased filling factor that reduces the dispersion in mass loading that occurs in the shock.

2.2 Flow in a galactic potential

The galactic potential we use is a combination of a two-armed spiral potential taken from Cox & Gomez (2002) of amplitude $n = 1 \text{ atom cm}^{-3}$, and a logarithmic potential (eg. Binney & Tremaine 1987) that provides a flat rotation curve with $v = 200 \text{ km/s}$. The spiral arms rotate as a fixed potential with pattern speed $2 \times 10^{-8} \text{ rad yr}^{-1}$. In addition to the main scientific simulations, we perform a number of control simulations in which self-gravity, or alternatively the fluid shock, are turned off in order to assess the physical importance of each in our results. The simulations were carried out on the United Kingdom’s Astrophysical Fluids Facility (UKAFF), a 128 CPU SGI Origin 3000 supercomputer.

2.2.1 Test particle simulation and the SPH initial conditions

The initial positions of particles in the spiral hydrodynamic simulations were taken from a test-particle simulation of orbits in the galactic potential. The particles were initially placed on tangential orbits with kinetic energies adapted from circular orbits so as to be consistent with the spiral potential together with an additional 5 % dispersion. They

Table 1.

Sim	$\Sigma (M_{\odot} \text{pc}^{-2})$	Mass (M_{\odot})	Npart
A	1	10^6	4.3×10^5
B	0.1	10^5	4.3×10^5
C	1	1.5×10^5	2.5×10^6

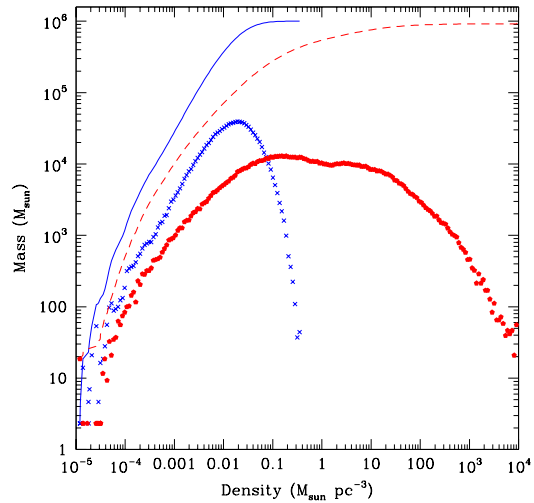


Figure 3. The distribution of mass as a function of gas density (points) is plotted before passing through the spiral shock (crosses) and once star formation has been triggered (filled pentagons) for Simulation A. The corresponding cumulative distributions are shown as the solid and dashed lines.

were then allowed to evolve over several orbits. The location of a significant density peak of size 100 pc in the spiral arm, at a galactic radius of $\approx 4 \text{ kpc}$, was chosen to identify ≈ 48000 test particles of interest. The earlier positions of these particles, before entering the spiral arm, were then used to establish the initial conditions of the SPH simulations. These test particles were given an additional 5 km/s Gaussian vertical velocity dispersion and then each subdivided into 9 SPH particles to provide the required resolution of 4.3×10^5 SPH particles. These initial conditions were used for our simulations. There are three scientific simulations which we discuss here, listed in Table 1. The first, Simulation A, uses the full initial conditions but with particle masses chosen to provide a mean surface density of $\Sigma = 1.0 M_{\odot} \text{ pc}^{-2}$ and a total mass of $10^6 M_{\odot}$. The second, Simulation B, is identical except for a lower surface density of $\Sigma = 0.1 M_{\odot} \text{ pc}^{-2}$ and total mass of $10^5 M_{\odot}$. The third, Simulation C, uses only the central region of the above initial conditions and then each particle is subdivided further, providing a higher resolution simulation of 2.5×10^6 SPH particles and a mass of $1.55 \times 10^5 M_{\odot}$ and $\Sigma = 1.0 M_{\odot} \text{ pc}^{-2}$. All subdivided particles had the same kinematics as the original particles.

The gas is initially clumpy on scales of several pc with a mean surface density of $1 M_{\odot} \text{ pc}^{-2}$, a volume-averaged density of $2.5 \times 10^{-3} M_{\odot} \text{ pc}^{-3}$, a median particle density of

$10^{-2} M_{\odot} \text{pc}^{-3}$ and peak densities in the clumps of $\approx 0.1 M_{\odot} \text{pc}^{-3}$ (See Figure 3). This clumpiness corresponds roughly to the properties of the interarm gas (Dickey & Lockman 1990). Self-gravity is initially unimportant due to the large shear velocities. For simplicity, the gas temperature was taken to be 100 K and remains isothermal throughout the simulation. This corresponds to a sound speed in molecular gas of 0.6 km/s. We consider that the gas is either in pre-existing molecular cloudlets (Pringle et al. 2001) or that molecular formation is sufficiently rapid as to occur in the shock compression (Bergin et al. 2004).

2.2.2 Sink particles and star formation

Star formation is modeled by the inclusion of sink-particles (Bate, Bonnell & Price 1995) that interact only through self-gravity and through accretion of any gas particles that fall within their sink radii. Sink-particle creation occurs when dense clumps ($\rho > 10^{-18} \text{g cm}^{-3}$, $1.4 \times 10^3 M_{\odot} \text{pc}^{-3}$) of self-gravitating gas of size ≤ 0.5 parsecs are collapsing (sub-virial). It should be noted that while the internal velocity dispersion of these regions is probably underestimated as the particles all lie inside one to two SPH kernels, the chosen temperature of 100K mimics the internal support expected for lower temperature gas with supersonic motions. This ensures that the star formation modeled here is real. The sink-particles have initial (minimum) masses of order 25 to 100 M_{\odot} and therefore cannot be considered as individual stars but can be thought of instead as stellar clusters. Accretion quickly increases the mass of these 'clusters' to 10^2 to $10^3 M_{\odot}$ with maximum masses of $m \approx 10^4 M_{\odot}$. The detailed computation of star formation within these clusters is beyond the scope of these investigations.

3 TRIGGERING OF STAR FORMATION IN THE SPIRAL SHOCK

The evolution of the gas over 34 million years as it passes through the spiral potential is shown in Figure 4 for Simulation A with an initial surface density of $\Sigma = 1 M_{\odot} \text{pc}^{-2}$. The initially clumpy, low density gas ($\rho \approx 0.01 M_{\odot} \text{pc}^{-3}$, $10^{-24} \text{g cm}^{-3}$) is compressed by the spiral shock as it leaves the minimum of the potential. The shock forms some very dense regions, which due to the accompanying dissipation of kinetic energy and the increased importance of self-gravity, can become gravitationally bound and thus collapse to form regions of star formation. These regions, in excess of $10^3 M_{\odot} \text{pc}^{-3}$ are replaced by sink particles. Further accretion onto the sink particles raises their masses to that of typical stellar clusters (10^2 to $10^4 M_{\odot}$). Star formation occurs within 2×10^6 years after sufficient densities are reached for the gas to be recognised as a molecular cloud (10^{-22} to $10^{-21} \text{g cm}^{-3}$). The total spiral arm passage lasts for $\approx 2 \times 10^7$ years. The gas remains globally unbound throughout the simulation and re-expands in the post-shock region.

In our simulations, the total fraction of gas turned into stars varies from between 5 and 30 % depending on the simulation, total gas mass and surface density. In reality this is likely to be an upper limit since there are other mechanisms not included in our computations such as the effects of winds and radiation from massive stars and supernova

explosions. We find that the total lifetime of the molecular clouds, measured from the time that significant mass attains typical GMC densities of 10^{-22} to $10^{-21} \text{g cm}^{-3}$, to be of order 10^7 years, or a few dynamical times ($t_{dyn} \approx 4 \times 10^6$ years).

The shock dissipation in the spiral arm is essential to trigger the star formation process. We have also run simulations that exclude the shock (with no SPH artificial viscosity) but include self-gravity; in these we find that there is no induced star formation even with orbit crowding and the increased importance of self-gravity in the spiral arms. Similarly, in Simulation B which is a full fluid simulation with but with a lower initial surface density of $\Sigma = 0.1 M_{\odot} \text{pc}^{-2}$, only limited star formation occurs, producing two 'star clusters' before the gas leaves the spiral arm and disperses. Triggering of star formation thus requires both the dissipation of the excess kinetic energy in the shearing flow and a critical threshold in surface density in order for self-gravity to become important.

In addition to forming dense clouds in which star formation occurs, the spiral shock forms structures which resemble the observed structures in GMCs. Detailed images of the GMCs formed in a spiral shock are shown in Figure 5 from Simulation C, with the gas density as in Simulation A, but at higher resolution simulation with $1.5 \times 10^5 M_{\odot}$ of gas, $\Sigma = 1 M_{\odot} \text{pc}^{-2}$, modelled with 2.5×10^6 SPH particles. The projections of the dense gas along a length of 50 pc, viewed from within and from above the disc of the galaxy, are taken just after star formation has been initiated. We see significant amounts of substructure as the dense gas breaks up into many components of several parsecs in size and separation. The dense regions have column densities typical to GMCs. This structure can be understood as being due to the combination of the clumpy nature of the pre-shock gas along with Rayleigh-Taylor like instabilities which occur as gas continues to flow into the shock.

4 THE GENERATION OF THE INTERNAL VELOCITY DISPERSION

One of the most significant properties of GMCs is their supersonic internal motions generally characterised by the internal velocity dispersion (Larson 1981; Heyer & Brunt 2004). Thus, in addition to triggering star formation, any mechanism to explain the formation of GMCs must be able to explain the origin of the internal velocity dispersion and how it depends on the size of the cloud, or region considered (Larson 1981; Heyer & Brunt 2004). Here we discuss how spiral triggering of star formation produces these kinematics when the pre-shock gas is clumpy. The basic idea is that when structure exists in the pre-shocked gas, the stopping point of a particular clump depends on the density of gas with which it interacts. Thus some regions will penetrate further into the shock, broadening it and leaving it with a remnant velocity dispersion in the shock direction. The different elements of the gas pass through shocks of different strengths and different orientations. The amount of mass-loading, and hence deceleration that occurs in the shock is variable due to the clumps in the pre-shock gas. Smaller scale regions in the shock are likely to have more correlated momentum injection as well as mass loading and thus small

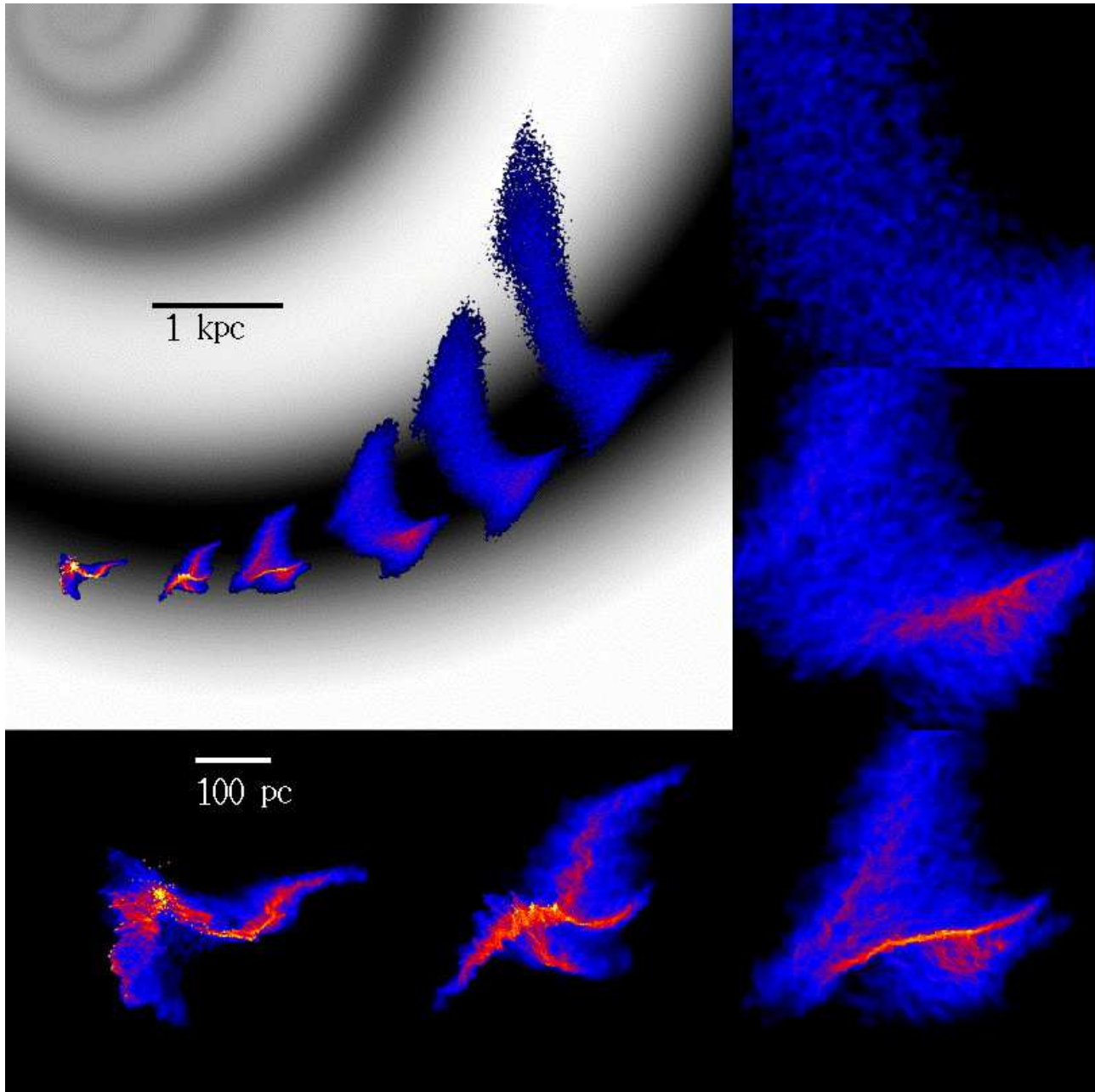


Figure 4. The evolution of cold interstellar gas ($m = 10^6 M_\odot$) through a spiral arm is shown relative to the spiral potential of the galaxy (upper left-panel) for Simulation A.. The minimum of the spiral potential is shown as black and the overall galactic potential is not shown for clarity. The column densities of the gas vary from 5×10^{-5} to 0.5 g cm^{-2} . The gas is shown at times $t = 9 \times 10^5$, $t = 9 \times 10^6$, $t = 1.8 \times 10^7$, $t = 2.3 \times 10^7$, $t = 2.8 \times 10^7$ and $t = 3.4 \times 10^7$ years from the start of the simulation. The 5 additional panels, arranged clockwise, show close-ups of the gas at the latter five times. The gas is compressed in the shock and subregions become self-gravitating and collapse to form groups of stars (from $t = 2.3 \times 10^7$ years). The cloud produces stars inefficiently as the gas is not globally bound.

velocity dispersions. Larger regions will have less correlation in both the momentum injection and mass loading such that there will be a larger dispersion in the post-shock velocity. Furthermore, the spiral potential ensures that the gas follows converging streams into the spiral shock such that there is a significant velocity component present parallel to the shock front. Together, this imparts a significant velocity dispersion in the post-shocked gas.

The evolution of the velocity dispersion in Simulation A as a function of the size of the region considered is shown

in Figure 6. The velocity dispersion is calculated from the velocity components in the plane of the galaxy within a spherical (3-D) region, and then normalised to produce a one-dimensional velocity dispersion, as would be observed. The velocity dispersion is then averaged over multiple regions of the same size all of which are centred on dense gas ($\rho \geq 10^{-21} \text{ g cm}^{-3}$). We only use particles whose densities exceed a minimum value of ($n \geq 10 \text{ cm}^{-3}$; $\rho \geq 1.7 \times 10^{-23} \text{ g cm}^{-3}$) to ensure we only consider the gas that has entered the shock. Lower density gas, even if molecular, is unlikely

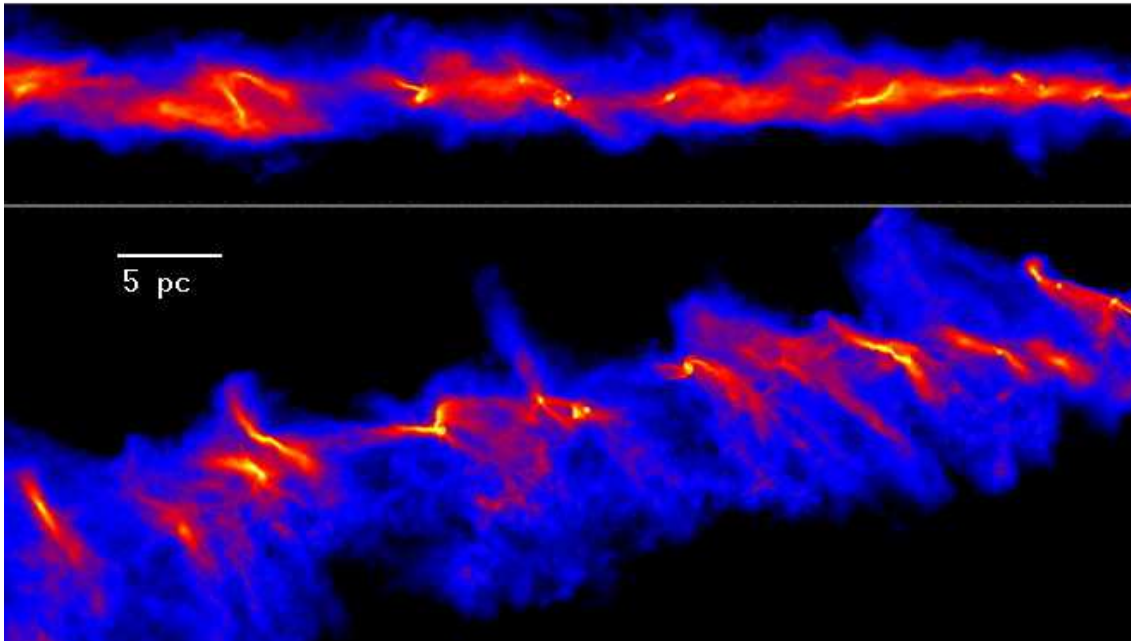


Figure 5. A 50 parsec region of the dense gas in the spiralshock is shown in two projections, from within the disc of the galaxy (upper panel) and from above the disc (lower panel), taken from a simulation of $3 \times 10^5 M_\odot$ modelled with 2.5×10^6 SPH particles. The gas has fragmented into many quasi-periodically-spaced dense regions with on-going star formation. The fragmentation occurs due to the clumpiness of the pre-shock gas and due to Rayleigh-Taylor like fluid instabilities in the shock. Column densities of the gas vary between 5×10^{-4} and 1 g cm^{-2} .

to excite any line emission. The initially low velocity dispersion, of order the sound speed $v_s \approx 0.6 \text{ km/s}$, increases as the gas passes through the spiral shock. At the same time, the velocity dispersion increases more on larger scales than on smaller scales thus establishing a velocity dispersion size-scale relationship which is approximately

$$v_{\text{disp}} \approx 1 \left(\frac{R}{1 \text{ pc}} \right)^{1/2} \text{ km/s.} \quad (2)$$

By the time that star formation has been triggered, the gas contains the characteristic kinematics of giant molecular clouds. The passage of the clumpy gas through the shock produces both the power-law slope and the magnitude of the velocity dispersion.

In the spiral shock, there is no distinction between the velocity dispersion inside a given cloud and the *intercloud* velocity dispersion. Thus, presumably the intercloud velocity dispersion in the spiral shock will follow the same sizescale relation. Once the clouds have passed through the shock they expand, with a simultaneous decrease in the internal velocity dispersion due to the dissipation of kinetic energy in the internal shocks. The velocity dispersion maintains a $R^{1/2}$ scaling but the magnitude decreases. Such clouds, if observed, should somewhat decrease the slope of the intercloud velocity dispersion sizescale relation. The caveat on this being that such clouds are likely to be increasingly difficult to detect in this epoch due to their decreasing surface densities.

This driving of the internal velocity dispersion due to the spiral shock occurs even for simulations where self-

gravity is not included. We can thus exclude that the velocity dispersion in our simulations is simply a reflection of the virialised nature of self-gravitating clouds. These clouds can be far from virialised, in fact completely unbound, and still display the same velocity dispersion. Thus we can fully attribute the generated velocity dispersion, and its dependency on the length scale considered, to the passage of the clumpy gas through the spiral shock.

5 DISCUSSION

The scenario presented here, of a dynamical triggering of star formation by the passage of inhomogeneous interstellar gas through a spiral shock, is consistent with the emergent viewpoint that star formation is a relatively fast process whereby clouds form out of the ISM, produce stars and then disperse, all on their local dynamical, or crossing, times (Elmegreen 2000; Hartmann et al. 2001). Few GMCs are observed without ongoing star formation suggesting that star formation must occur soon after the clouds form. Estimates based on the ages and distribution of young stellar populations imply that star formation itself occurs on a dynamical timescale (Elmegreen 2000) while the lack of molecular gas around older systems suggest that the clouds disperse after at most a few dynamical timescales (Leisawitz et al. 1989). From our simulations we estimate lifetimes of the dense clouds of order 10^7 years, or a few dynamical times ($t_{\text{dyn}} \approx 4 \times 10^6$ years), with pre-star formation lifetimes of order 2×10^6 years. We find star formation efficiencies in the

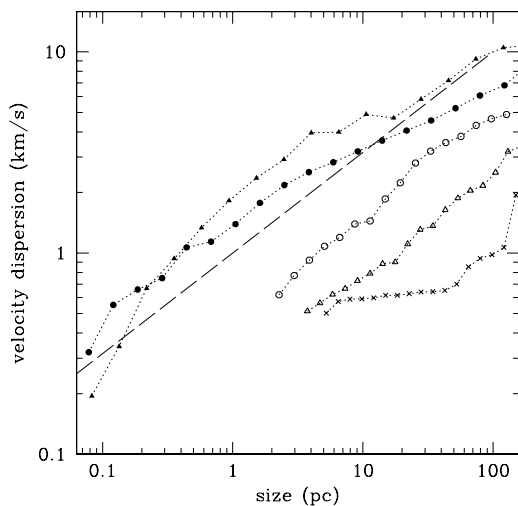


Figure 6. The velocity dispersion is plotted as a function of size at 5 different times during the passage of the gas through a spiral shock (Simulation A). The velocity dispersion is plotted at 4.2×10^6 years (crosses), 1.4×10^7 years (open triangles), 1.8×10^7 years (open octagans), 2.3×10^7 years (filled circles) and 2.7×10^7 years (filled triangles) after the start of the simulation. Star formation is initiated at $\approx 2.3 \times 10^7$ years. The velocity dispersion is calculated from the velocities in the plane of the disc, which are then averaged over many different regions of a given size that each have central gas densities in excess of $10^{-21} \text{ g cm}^{-3}$. The dashed line indicates the Larson relation for molecular clouds where $\sigma \propto R^{-1/2}$ (Larson 1981; Heyer & Brunt 2004).

range 5–30 percent, but note that these are likely to be reduced by including the effects of feedback from young stars and/or magnetic fields.

Our simulations also demonstrate that the observed internal kinematics of GMCs can be caused simply by the passage of an initially clumpy ISM through the spiral shock. There is then no need for any internal or external driving mechanism for the ‘turbulence’ in terms of magnetic instabilities, gravitational instabilities, stellar outflows, winds or supernovae (Mac Low & Klessen, 2004). The velocity dispersion is generated at all scales simultaneously (Brunt 2003) and thus no turbulent cascade of energy from larger to smaller lengthscales is required. Once generated, these internal motions are likely to evolve as in simulations of decaying supersonic turbulence (Mac Low et al. 1998). A caveat to this notion of decaying turbulence is that only 25 per cent of the gas in the dense clouds has centre of mass motions with radii of curvature of 10 pc or less. Thus the majority of the internal motions in the dense clouds do not show evidence for significant eddy motions on sizescales of molecular clouds.

Furthermore, we have seen that GMCs do not need be globally gravitationally bound in order to explain their properties or their evolution. This relaxation of a generally held assumption (that the GMCs are in virial equilibrium) permits a straightforward explanation for the low star formation efficiency in GMCs. The vast majority of the gas is never gravitationally bound and thus does not undergo star formation. Local regions in unbound clouds can dissipate suf-

ficient kinetic energy to become gravitationally bound and thus collapse to form stars (Clark & Bonnell 2004). These regions then provide the initial conditions for detailed studies of the star formation process (Bate, Bonnell & Bromm 2003; Bonnell, Bate & Vine 2003). A recent simulation of an unbound GMC has shown that star formation efficiencies on the order of 10 per cent are a natural outcome of the unbound nature of the clouds (Clark et al. 2005).

Although our models are explicitly made with two-armed grand-design spiral features, the spiral shock origin for star formation could equally apply to flocculent spiral galaxies. In such systems any gravitational instabilities will be sheared into local spiral arms (Elmegreen, Elmegreen & Leitner 2003) as occurs in any weakly self-gravitating disc (Rice et al. 2003). Shocks due to the passage of gas through these spiral arms can then trigger star formation much in the way described in this paper.

5.1 Comparison with observations

Detailed comparisons with observations of spiral galaxies (Tilanus & Allen 1993; Allen et al. 1997; Smith et al. 2000; Schinnerer et al. 2003) will require global disc calculations (Dobbs et al., in preparation) and should ideally include more physical processes such as a realistic equation of state, feedback from young stars, and the effects of magnetic fields. Notwithstanding, there are several predictions from this scenario which can be tested observationally.

First, the mechanisms detailed here is of a clumpy gas that forms GMCs due to the passage through a spiral shock. The implication is that GMCs should reside primarily in spiral arms of galaxies. This is consistent with surveys of the outer Galaxy (Heyer et al. 1998) which finds an arm-interarm density ratio of GMCs in the Perseus arm to be 28:1 (Heyer & Terebey 1998). The overall distribution of GMCs in the outer galaxy also reinforces the impression that they are confined to spiral arms (Heyer, personal communication)¹. The global distribution of CO gas in the Galaxy is also best explained as being predominantly in spiral arms (Bissantz, Englmaier & Gerhard 2003).

Second, the internal velocity dispersion is driven primarily at the shock itself. Therefore the gas should have relatively low internal velocity dispersions prior to the shock that increase rapidly at the shock front and decay monotonically thereafter.

Third, the strength and scaling relations of the velocity dispersion should be independent of the proximity of young stars or other potential sources of turbulence. This appears to be the case in the Carina giant molecular cloud (Zhang et al. 2001).

Fourth, the shock-driven origin of the GMCs implies that they should have sharper edges on the upwind side where fresh material is flowing into the shock, while the downwind edge to the GMCs is smoother due to the gas dispersal. This can be seen in Figure 5.

Fifth, a potential implication of this work is that at least some component of the the velocity dispersion seen

¹ The presence of GMCs in spiral arms is, at least in our Galaxy, not surprising as the spiral arms are generally defined by the presence of star formation and hence of star forming GMCs.

in the inter-arm gas (Dickey & Lockman 1990) is due to this pumping process in the spiral arms. The structure and kinematics that result from the spiral shock should then feed directly into the next spiral passage.

6 CONCLUSIONS

The triggering of star formation by the passage of clumpy gas through a spiral arm can explain many of the observed properties of star forming regions. The clumpy shock reproduces the observed kinematics of GMCs, the so-called 'Larson' relation. There is no need for any internal driving of the quasi-turbulent random motions. The shock forms dense structures in the gas which become locally bound and collapse to form stars. The clouds are globally unbound and thus disperse on timescales of 10^7 years, resulting in relatively low star formation efficiencies.

ACKNOWLEDGMENTS

The computations reported here were performed using the U.K. Astrophysical Fluids Facility (UKAFF). We thank Bruce Elmegreen, Mark Heyer, Chris Brunt and the referee John Scalo for helpful comments.

REFERENCES

- Allen R. J., Knapen J. H., Bohlin R., Stecher T. P., 1997, ApJ, 487, 171
- Baade, W., 1963, Evolution of stars and Galaxies, Harvard University press (Cambridge), p 63.
- Bash F. N., Green E., Peters W. L., 1977, ApJ, 217, 464
- Bate M. R., Bonnell I. A., Price N. M., 1995, MNRAS, 277, 362.
- Bate M. R., Bonnell I. A., Bromm V., 2003, MNRAS, 339, 577
- Benz W., Bowers R. L., Cameron A. G. W., Press B., 1991, ApJ, 348, 647.
- Bergin E. A., Hartmann L. W., Raymond J. C., Ballesteros-Paredes J., 2004, ApJ, 612, 921
- Binney, J., & Tremaine, S., 1987, Galactic Dynamics, Princeton U. Press
- Blitz, L., Rosolowsky E., 2004, ApJL, 612, L29
- Blitz, L., Shu F.H., 1980 ApJ, 238, 148
- Blitz, L. & Williams, J., 1999, *The origin of stars and planetary systems*, eds C.J.Lada, N.D. Kylafis, (Kluwer:Dordrecht), 3
- Bonnell I. A., Bate M. R., Vine S. G., 2003, MNRAS, 343, 413
- Bonnell I. A., Clarke C. J., Bate M. R., Pringle J. E., 2001, MNRAS, 324, 573.
- Brunt, C.M., 2003, ApJ, 583, 280
- Clark, P.C., Bonnell, I.A., 2004 MNRAS, 347, L36
- Clark, P.C., Bonnell, I.A., Zinnecker, H., Bate, M.R., 2004 MNRAS, submitted ,
- Clarke C.J., Bonnell I. A., Hillenbrand L. A., 2000, , in Protostars and Planets IV (eds V. Mannings, A. P. Boss and S. Russell), 151.
- Cowie L. L., 1981, ApJ, 245, 66
- Cox, D.P., Gomez, G.C., 2002., ApJS, 142, 261
- Dickey, J. M., Lockman, F.J., H I in the Galaxy, ARA&A, f 28, 215-261, (1990).
- Drimmel, R., Spergel, D.N., 2001, ApJ, 556, 181
- Elmegreen B. G., 1979, ApJ, 231, 372
- Elmegreen B. G., 1991, ApJ, 378, 139
- Elmegreen B. G., 1993, ApJ, 411, 170
- Elmegreen B. 2000, ApJ, 530, 277
- Elmegreen B. G., Elmegreen D. M., 1983, MNRAS, 203, 31
- Elmegreen B. G., Elmegreen D. M., Leitner S. N., 2003, ApJ, 590, 271
- Elmegreen B., Scalo, J., 2004, ARA&A, 42, 211
- Heyer M. H., Brunt C. M., Snell R.L., Howe J.E., Schloerb F.P., 1998, ApJ,S, 115, 241
- Heyer M. H., Brunt C. M., 2004, ApJ, 615, 45
- Heyer M. H., Schloerb F. P., 1997, ApJ, 475, 173
- Heyer M. H., Terebey S., 1998, ApJ, 502, 265
- Ferguson A. M. N., Wyse R. F. G., Gallagher J. S., Hunter D. A., 1998, ApJ, 506, L19
- Hartmann, L., Ballesteros-Paredes, J., Bergin, E.A., 2001, ApJ, bf 562, 852
- Kornreich, P., and Scalo, J., 2000, ApJ, 531 366
- Larson R. B., 1981, MNRAS, 194, 809.
- Larson, R.B., 2003, Rep. Prog. Physics, 66, 1651
- Lauroesch, J.T., Meyer, D.M., Blades, J.C., 2000, ApJ, 543, L43
- Leisawitz, D., 1990, ApJ, 359, 319
- Leisawitz, D., Bash, F.N., Thaddeus, P., 1989, ApJS, 70, 731
- Lubow, S.H.; Pringle, J.E. 1996, MNRAS, 279, 1251
- Mac Low M., Klessen R. S., Burkert A., Smith M. D., 1998, PhRvL, 80, 2754
- Mac Low, M.M., Klessen, R.S., 2004, RvMP, 74, 125
- Miesch, M.S.; Bally, J., 1994., ApJ, 429, 645
- Monaghan J. J., 1992, ARA&A, 30, 543.
- Motte F., André P., Neri R., 1998, A&A, 336, 150
- Pringle, J.E., Allen, R.J., Lubow, S.H., 2001., MNRAS, 327, 663
- Rice W. K. M., Armitage P. J., Bate M. R., Bonnell I. A., 2003, MNRAS, 338, 227
- Roberts, W.W., 1969, ApJ, 158, 123
- Rumstay K. S., Kaufman M., 1983, ApJ, 274, 611
- Schinnerer, E., Weiss, A., Scoville, N.Z., Aalto, S., 2003, IAU Symp. no. 221, 145
- Schweizer F., 1976, ApJS, 31, 313
- Seigar, M.S., James, P.A. 2002, MNRAS, 337, 1113
- Silk J., 1985, ApJ, 292, L71
- Smith D. A., Allen R. J., Bohlin R. C., Nicholson N., Stecher T. P., 2000, ApJ, 538, 608
- Tennekes H., Lumley J., 1972, MIT Press
- Tilanus R. P. J., Allen R. J., 1993, A&A, 274, 707
- van den Bergh S., 1964, ApJS, 9, 65
- Wada, K., Koda J., 2004, MNRAS, 349, 270
- Wada, K., Norman, C., 2001, 547, 172
- Williams J. P., Blitz L., McKee C. F., 2000, prpl.conf, 97
- Zhang, X., Lee, Y., Bolatto, A., Stark, A.A., 2001, ApJ, 553, 274
- Zuckerman, B., Evans, N.J., 1974, apj, 192, L149